

# Chemical clocks for early-type galaxies in clusters

Conrado Carretero<sup>1</sup>, Alexandre Vazdekis<sup>1</sup> and John E. Beckman<sup>1,2</sup>

<sup>1</sup>Instituto de Astrofísica de Canarias. 38200 La Laguna, Tenerife, Spain. Email: cch@iac.es

<sup>2</sup>Consejo Superior de Investigaciones Científicas, Spain.

**Abstract.** We present a detailed stellar population analysis of 27 massive elliptical galaxies within 4 very rich clusters at redshift  $z \sim 0.2$ . We obtained accurate estimates of the mean luminosity-weighted ages and relative abundances of CN, Mg and Fe as functions of the galaxy velocity dispersion,  $\sigma$ . Our results are compatible with a scenario in which the stellar populations of massive elliptical galaxies, independently of their environment and mass, had formation timescales shorter than  $\sim 1$  Gyr. This result implies that massive elliptical galaxies have evolved passively since, at least, as long ago as  $z \sim 2$ . For a given galaxy mass the duration of star formation is shorter in those galaxies belonging to more dense environments. Finally, we show that the abundance ratios [CN/Fe] and [Mg/Fe] are the key “chemical clocks” to infer the star formation history timescales in ellipticals. In particular, [Mg/Fe] provides an upper limit for those formation timescales, while [CN/Fe] appears to be the most suitable parameter to resolve them in elliptical galaxies with  $\sigma < 300$  km s<sup>-1</sup>.

**Keywords.** galaxies: abundances, galaxies: clusters: general, galaxies: elliptical and lenticular, cD, galaxies: evolution, galaxies: formation

---

## 1. Introduction

Stellar Population analysis has recently shown increasing power in constraining galaxy formation scenarios. They offer a fossil record of the star formation and chemical evolution of galaxies, most clearly in elliptical galaxies, thought to have formed by the merging of discs, so stellar population studies provide very strong constraints on these galaxy formation scenarios. For example, it is particularly hard to reconcile the hierarchical models with the result that massive galaxies show significantly older mean luminosity weighted ages than their smaller counterparts (Kauffmann et al. 2003).

A key point is to see how abundance ratios in early-type galaxies vary with the cluster masses. In particular, overabundances of [Mg/Fe] compared with the solar ratio have been found in massive elliptical galaxies (e.g. Vazdekis et al. 1997). In this work, we concentrate on the stellar population analysis of 27 elliptical galaxies distributed in 4 rich, intermediate-redshift ( $z \sim 0.2$ ) Abell clusters.

## 2. Observations and Data

We have studied a set of 27 elliptical galaxies belonging to 4 very rich Abell clusters: A115, A655, A963 and A2111. The selected galaxies are the brightest galaxies in their respective clusters ( $15.1 < m_V < 17.2$ ) and have been already morphologically analyzed in the literature. The velocity dispersion covers the range  $220 \text{ km s}^{-1} < \sigma < 450 \text{ km s}^{-1}$ .

Multi-slit spectroscopy was carried out with the DOLORES spectrograph on the 3.5m TNG Telescope (La Palma). We designed MOS masks with  $1.1''$  width slits and an instrumental resolution of  $8 \text{ \AA}$  (FWHM).

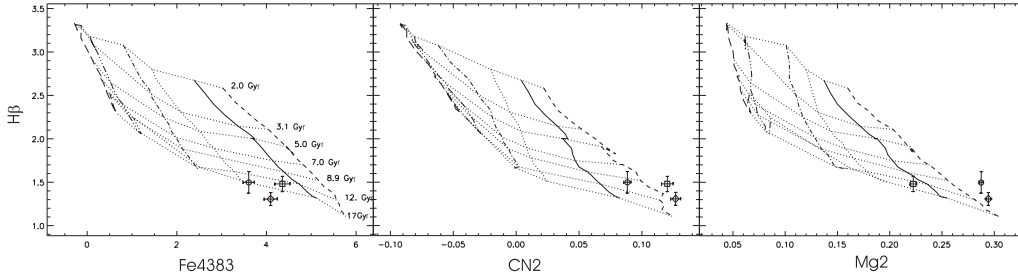


**Figure 1.** Examples of the method used to derive ages and metallicities. The plot shows the age index  $H\beta$  versus the metallicity indicators Fe4383, CN2 and  $Mg_2$  for the grid of models of Vazdekis et al. (2006, in preparation). Horizontal dotted lines represent models of constant age whose ages are labelled in the plot. Vertical dashed, solid, dotted, dashed-dotted, dashed-dotted-dotted and long-dashed lines represent contours of constant  $[M/H] = +0.2, 0.0, -0.4, -0.7, -1.2$  and  $-1.7$  dex, respectively. Diamonds, open circles and squares indicate the values for a representative galaxy of A115, A655 and A963, respectively, with a common  $\sigma = 310 \text{ km s}^{-1}$ . Note that all synthetic model spectra were broadened to the instrumental resolution of the observed spectra and the velocity dispersion of these particular galaxies ( $\sigma_{\text{obs}} = 350 \text{ km s}^{-1}$ ).

### 3. Analysis

To derive mean luminosity-weighted ages and metallicities, we compared selected absorption line strengths with those predicted by the model of Vazdekis et al. (2006, in preparation). This model provides flux-calibrated spectra in the wavelength range  $\lambda\lambda 3500\text{-}7500 \text{ \AA}$ , at a resolution of  $2 \text{ \AA}$  (FWHM) for single-burst stellar populations.

Once the model spectra are transformed to yield the instrumental conditions of resolution and dispersion of the observed spectrum, we measure pairs of indices in both sets of data (observed and synthetic). Figure 1 illustrates this method.

### 4. Results

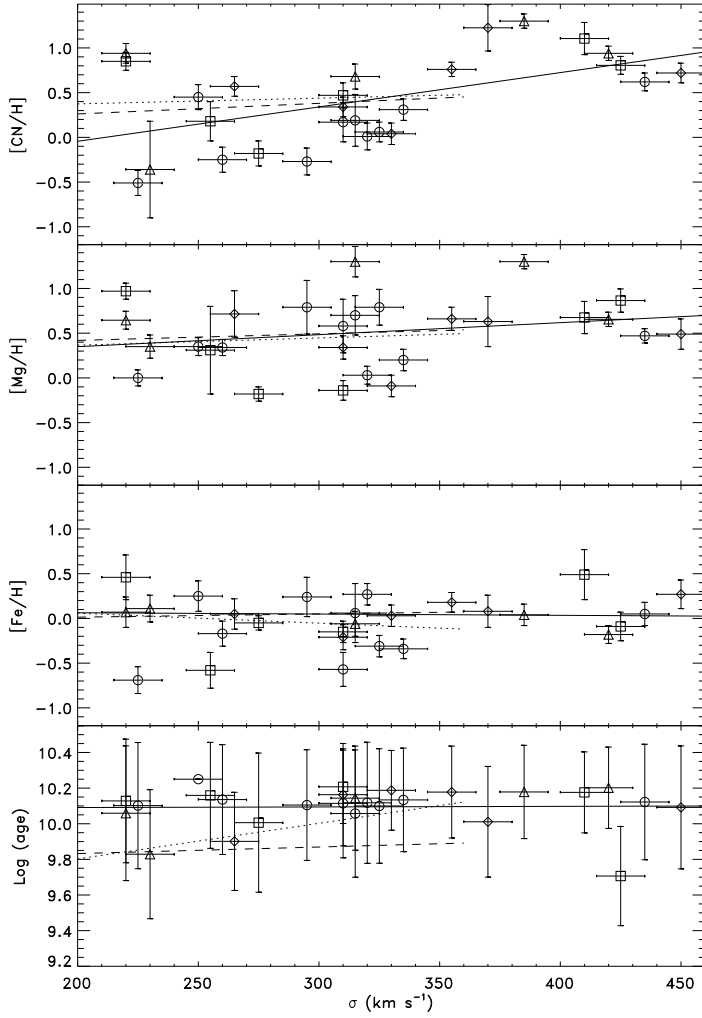
Figure 2 presents the relations  $[\text{CN}/\text{H}]-\sigma$ ,  $[\text{Mg}/\text{H}]-\sigma$ ,  $[\text{Fe}/\text{H}]-\sigma$  and  $\text{Log}(\text{age})-\sigma$  for our full sample. We have also plotted on Figure 2 the results obtained by Sánchez-Blázquez et al. (2006), who analyzed 98 early-type galaxies of the Virgo and Coma clusters.

Figure 3 presents the relations of the abundance ratios  $[\text{CN}/\text{Fe}]$  and  $[\text{Mg}/\text{Fe}]$  with the velocity dispersion. We observe positive trends with  $\sigma$  for both ratios.

### 5. Discussion

First, when inspecting Figures 2 and 3 we observe that, for a given  $\sigma$ , the relative abundance  $[\text{CN}/\text{H}]$  increases with the cluster X-ray luminosity, whereas  $[\text{Mg}/\text{H}]$  and  $[\text{Fe}/\text{H}]$  do not. The same happens with the abundance ratios: while  $[\text{CN}/\text{Fe}]$  increases as a function of the environment density, the  $[\text{Mg}/\text{Fe}]$  ratio keeps constant and *positive*.

If we consider the formation timescales for Mg and Fe we can estimate that, whatever the environment is, all stellar populations in ellipticals should be already formed in less than  $\sim 1 \text{ Gyr}$ , since this is the time needed by SNe Ia to pollute the ISM with iron-peak elements. But, if we consider species with less separated formation timescales, such as Fe and CN, we do find differences in the ratio  $[\text{CN}/\text{Fe}]$  as a function of the environment, for a given  $\sigma$ . That suggests a different formation timescale for the stars in ellipticals related to the environment properties, in the sense that the more dense the environment is the shorter the formation timescales of the stars are (with an upper limit of  $\sim 1 \text{ Gyr}$ ). This



**Figure 2.** Relations between the relative abundances  $[CN/H]$ ,  $[Mg/H]$ ,  $[Fe/H]$ , and mean luminosity-weighted ages and the velocity dispersion of the galaxies,  $\sigma$ . Diamonds: A115 galaxies. Open circles: A655 galaxies. Open squares: A963 galaxies. Open triangles: A2111 galaxies. The solid line corresponds to the error-weighted linear fitting to our data. Dotted line and dashed line corresponds to the relations obtained for Virgo cluster galaxies and Coma cluster galaxies, respectively. It is noteworthy that the slope of the relations increases with the environment density for  $[CN/H]-\sigma$ , while it is almost constant in the case of  $[Mg/H]-\sigma$  and  $[Fe/H]-\sigma$ .

is in agreement with a number of recent results (e.g. Carretero et al. 2004, Thomas et al. 2005, Bernardi et al. 2006).

Second, it is noteworthy that the slope of the relation  $[CN/Fe]-\sigma$  increases with the cluster X-ray luminosity while the slope of the  $[Mg/Fe]-\sigma$  is constant with the cluster mass. Because of that, we can only find environment-related  $[CN/Fe]$  differences in those galaxies with  $\sigma < 300 \text{ km s}^{-1}$  whereas, for more massive galaxies, the  $[CN/Fe]$  values are almost equal independently of the cluster properties. This means that the ratio  $[CN/Fe]$  in most massive galaxies is less sensitive to the environment than in intermediate- and low-mass galaxies, suggesting that star formation histories are less environment dependent as the galaxy mass increases. Therefore,  $[CN/Fe]$  appears to be an appropriate “chemical

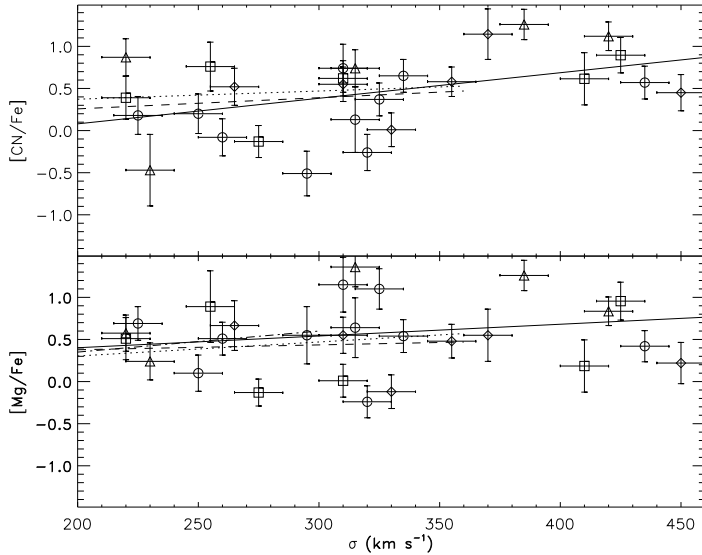


**Figure 3.** Abundance ratios  $[\text{CN}/\text{Fe}]$  and  $[\text{Mg}/\text{Fe}]$  versus the velocity dispersion of the galaxies. Symbols are the same than in previous Figure. Dashed-dotted line in bottom panel corresponds to the  $[\text{Mg}/\text{Fe}]-\sigma$  relation for Virgo cluster galaxies, by Vazdekis et al. (2004). Note that the slope of the  $[\text{CN}/\text{Fe}]-\sigma$  relation increases with the density of the environment, but the  $[\text{Mg}/\text{Fe}]-\sigma$  remains almost constant.

clock” for ellipticals with  $\sigma < 300 \text{ km s}^{-1}$  but, when we move to very massive galaxies, the formation timescales differ so gently from one environment to another that this “clock” turns out to be insufficiently sensitive. In order to disentangle the different formation timescales between very massive galaxies in different environments, it is necessary to find out a more accurate indicator.

Our results suggest an overall picture in which massive elliptical galaxies in very rich clusters are old systems, with very short star formation histories, and which have been passively evolving since, at least,  $z \sim 2$ . This is in agreement with a number recent results (e.g. Labé et al. 2005, van Dokkum et al. 2006). In comparison with less dense environments, the stars in elliptical galaxies of rich clusters must have formed at slightly earlier epochs and on a slightly shorter timescales.

### Acknowledgements

This work has been supported by the Spanish Ministry of Education and Science grants AYA2004-03059 and AYA2004-08251-C02-01.

### References

- Bernardi M., Nichol R. C., Sheth R. K., Miller C. J., Brinkmann J., 2006, *AJ*, 131, 1288
- Carretero C., Vazdekis A., Beckman J. E., Sánchez-Blázquez P., Gorgas J., 2004, *ApJ*, 609, L45
- Kauffmann G., et al., 2003, *MNRAS*, 341, 54
- Labbé I., et al., 2005, *ApJ*, 624, L81
- Sánchez-Blázquez P., Gorgas J., Cardiel N., González J. J., 2006, *A&A*, 457, 809
- Thomas D., Maraston C., Bender R., Mendes de Oliveira C., 2005, *ApJ*, 621, 673
- van Dokkum P. G., van der Marel R. P., 2006, *astro-ph/0603063*
- Vazdekis A., Peletier R. F., Beckman J. E., Casuso E., 1997, *ApJS*, 111, 203
- Vazdekis A., Trujillo I., Yamada Y., 2004, *ApJ*, 601, L33

# An interesting and seminal work on various phenomena in fluid mechanics

Alan N. Other<sup>1</sup>†, H.-C. Smith<sup>1</sup>  
and J.Q. Public<sup>2</sup>

<sup>1</sup>Department of Chemical Engineering, University of America, Somewhere, IN 12345, USA  
email: .....

<sup>2</sup>Department of Aerospace and Mechanical Engineering, University of Camford,  
Academic Street, Camford, CF3 5QL, UK  
email: .....

**Abstract.** Using Stokes flow between eccentric counter-rotating cylinders as a prototype for bounded nearly parallel lubrication flow, we investigate the effect of a slender recirculation region within the flow field on cross-stream heat or mass transport in the important limit of high Péclet number  $Pe$  where the ‘enhancement’ over pure conduction heat transfer without recirculation is most pronounced. The steady enhancement is estimated with a matched asymptotic expansion to resolve the diffusive boundary layers at the separatrices which bound the recirculation region. The enhancement over pure conduction is shown to vary as  $\epsilon^{1/2}$  at infinite  $Pe$ , where  $\epsilon^{1/2}$  is the characteristic width of the recirculation region. The enhancement decays from this asymptote as  $Pe^{-1/2}$ .

**Keywords.** Keyword1, keyword2, keyword3, etc.

---

## 1. Introduction

The use of integral equations to solve ‘exterior’ problems in linear acoustics, i.e. to solve the Helmholtz equation  $(\nabla^2 + k^2)\phi = 0$  outside a surface  $S$  given that  $\phi$  satisfies certain boundary conditions on  $S$ , is very common. A good description is provided by Martin (1980). Integral equations have also been used to solve the two-dimensional Helmholtz equation that arises in water-wave problems where there is a constant depth variation. The problem of wave oscillations in arbitrarily shaped harbours using such techniques has been examined (see for example Hwang & Tuck 1970; Lee 1971; Figer, Najarro, Gilmore, *et al.* (2002)).

In a recent paper Linton & Evans (1992) have shown how radiation and scattering problems for vertical circular cylinders placed on the centreline of a channel of finite water depth can be solved efficiently using the multipole method devised originally by Ursell (1950). This method was also used by Callan, Linton & Evans (1991) to prove the existence of trapped modes in the vicinity of such a cylinder at a discrete wavenumber  $k < \pi/2d$  where  $2d$  is the channel width.

Many water-wave/body interaction problems in which the body is a vertical cylinder with constant cross-section can be simplified by factoring out the depth dependence. Thus if the boundary conditions are homogeneous we can write the velocity potential  $\phi(x, y, z, t) = \text{Re}\{\phi(x, y) \cosh k(z + h)e^{-i\omega t}\}$ , where the  $(x, y)$ -plane corresponds to the undisturbed free surface and  $z$  is measured vertically upwards with  $z = -h$  the bottom of the channel.

Subsequently Callan *et al.* (1991) proved the existence of, and computed the wavenumbers for, the circular cross-section case. It should be noted however that experimental

† Present address: Fluid Mech Inc., 24 The Street, Lagos, Nigeria.

evidence for acoustic resonances in the case of the circular cylinder is given by Bearman & Graham (1980, pp. 231–232).

Koch (1983) provided a theory for determining the trapped-mode frequencies for the thin plate, based on a modification of the Wiener–Hopf technique. Further interesting results can be found in Williams (1964) and Dennis (1985).

The use of channel Green’s functions allows the far-field behaviour to be computed in an extremely simple manner, whilst the integral equation constructed in §3 enables the trapped modes to be computed in §4 and the scattering of an incident plane wave to be solved in §5. Appendix A contains comparisons with experiments. The Galactic Center region proves to be an area very rich in WR stars. The VIIth Catalogue lists within 50 pc from the Galactic Center 15 WNL and 11 WCL stars, at near-IR wavelengths discovered by Krabbe, Genzel, Eckart, *et al.* (1995) in the Galactic Center Cluster.

## 2. Green’s functions

### 2.1. Construction of equations

We are concerned with problems for which the solution,  $\phi$ , is either symmetric or anti-symmetric about the centreline of the waveguide,  $y = 0$ . The first step is the construction of a symmetric and an antisymmetric Green’s function,  $G_s(P, Q)$  and  $G_a(P, Q)$ . Thus we require

$$(\nabla^2 + k^2)G_s = (\nabla^2 + k^2)G_a = 0 \quad (2.1)$$

in the fluid, where  $\nabla$  is a gradient operator,

$$\nabla \cdot \mathbf{v} = 0, \quad \nabla^2 P = \nabla \cdot (\mathbf{v} \times \mathbf{w}).$$

In (2.1)

$$G_s, G_a \sim 1/(2\pi) \ln r \quad \text{as} \quad r \equiv |P - Q| \rightarrow 0, \quad (2.2)$$

$$\frac{\partial G_s}{\partial y} = \frac{\partial G_a}{\partial y} = 0 \quad \text{on} \quad y = d, \quad (2.3)$$

$$\frac{\partial G_s}{\partial y} = 0 \quad \text{on} \quad y = 0, \quad (2.4)$$

$$G_a = 0 \quad \text{on} \quad y = 0, \quad (2.5)$$

and we require  $G_s$  and  $G_a$  to behave like outgoing waves as  $|x| \rightarrow \infty$ .

One way of constructing  $G_s$  or  $G_a$  is to replace (2.1) and (2.2) by

$$(\nabla^2 + k^2)G_s = (\nabla^2 + k^2)G_a = -\delta(x - \xi)\delta(y - \eta) \quad (2.6)$$

and to assume initially that  $k$  has a positive imaginary part.

### 2.2. Further developments

Using results from Linton & Evans (1992) we see that this has the integral representation

$$-\frac{1}{2\pi} \int_0^\infty \gamma^{-1} [e^{-k\gamma|y-\eta|} + e^{-k\gamma(2d-y-\eta)}] \cos k(x - \xi)t \, dt, \quad 0 < y, \quad \eta < d, \quad (2.7)$$

where

$$\gamma(t) = \begin{cases} -i(1 - t^2)^{1/2}, & t \leq 1 \\ (t^2 - 1)^{1/2}, & t > 1. \end{cases}$$

In order to satisfy (2.4) we add to this the function

$$-\frac{1}{2\pi} \int_0^\infty B(t) \frac{\cosh k\gamma(d-y)}{\gamma \sinh k\gamma d} \cos k(x-\xi)t dt$$

which satisfies (2.1), (2.3) and obtain

$$B(t) = 2e^{-k\gamma d} \cosh k\gamma(d-\eta). \quad (2.8)$$

Thus the function

$$G = -\frac{1}{4}i(H_0(kr) + H_0(kr_1)) - \frac{1}{\pi} \int_0^\infty \frac{e^{-k\gamma d}}{\gamma \sinh k\gamma d} \cosh k\gamma(d-y) \cosh k\gamma(d-\eta) \quad (2.9)$$

satisfies (2.1)–(2.4). By writing this function as a single integral which is even in  $\gamma$ , it follows that  $G$  is real. Similar ideas have been developed in a variety of ways (Keller 1977; Rogallo 1981; van Wijngaarden 1968).

### 3. The trapped-mode problem

The unit normal from  $D$  to  $\partial D$  is  $\mathbf{n}_q = (-y'(\theta), x'(\theta))/w(\theta)$ . Now  $G_a = \frac{1}{4}Y_0(kr) + \widetilde{G}_a$  where  $r = \{[x(\theta) - x(\psi)]^2 + [y(\theta) - y(\psi)]^2\}^{1/2}$  and  $\widetilde{G}_a$  is regular as  $kr \rightarrow 0$ . In order to evaluate  $\partial G_a(\theta, \theta)/\partial n_q$  we note that

$$\frac{\partial}{\partial n_q} \left( \frac{1}{4}Y_0(kr) \right) \sim \frac{\partial}{\partial n_q} \left( \frac{1}{2\pi} \ln r \right) = \frac{1}{2\pi r^2 w(\theta)} [x'(\theta)(y(\theta) - y(\psi)) - y'(\theta)(x(\theta) - x(\psi))]$$

as  $kr \rightarrow 0$ . Expanding  $x(\psi)$  and  $y(\psi)$  about the point  $\psi = \theta$  then shows that

$$\begin{aligned} \frac{\partial}{\partial n_q} \left( \frac{1}{4}Y_0(kr) \right) &\sim \frac{1}{4\pi w^3(\theta)} [x''(\theta)y'(\theta) - y''(\theta)x'(\theta)] \\ &= \frac{1}{4\pi w^3(\theta)} [\rho'(\theta)\rho''(\theta) - \rho^2(\theta) - 2\rho'^2(\theta)] \quad \text{as } kr \rightarrow 0. \end{aligned} \quad (3.1)$$

#### 3.1. Computation

For computational purposes we discretize (3.1) by dividing the interval  $(0, \pi)$  into  $M$  segments. Thus we write

$$\frac{1}{2}\phi(\psi) = \frac{\pi}{M} \sum_{j=1}^M \phi(\theta_j) \frac{\partial}{\partial n_q} G_a(\psi, \theta_j) w(\theta_j), \quad 0 < \psi < \pi, \quad (3.2)$$

where  $\theta_j = (j - \frac{1}{2})\pi/M$ . Collocating at  $\psi = \theta_i$  and writing  $\phi_i = \phi(\theta_i)$  etc. gives

$$\frac{1}{2}\phi_i = \frac{\pi}{M} \sum_{j=1}^M \phi_j K_{ij}^a w_j, \quad i = 1, \dots, M, \quad (3.3)$$

where

$$K_{ij}^a = \begin{cases} \partial G_a(\theta_i, \theta_j)/\partial n_q, & i \neq j \\ \partial \widetilde{G}_a(\theta_i, \theta_i)/\partial n_q + [\rho'_i \rho''_i - \rho_i^2 - 2\rho_i'^2]/4\pi w_i^3, & i = j. \end{cases} \quad (3.4)$$

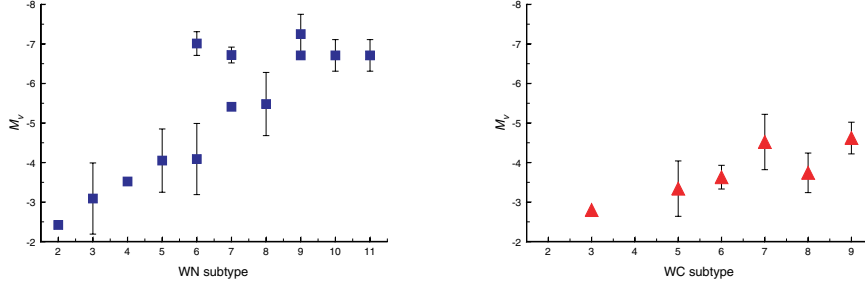
For a trapped mode, therefore, we require the determinant of the  $M \times M$  matrix whose elements are

$$\delta_{ij} - \frac{2\pi}{M} K_{ij}^a w_j,$$

to be zero. Table 1 shows a comparison of results obtained from this method using two

**Table 1.** Values of  $kd$  at which trapped modes occur when  $\rho(\theta) = a$ 

$a/d$	$M = 4$	$M = 8$	Callan <i>et al.</i>
0.1	1.56905	1.56	1.56904
0.3	1.50484	1.504	1.50484
0.55	1.39128	1.391	1.39131
0.7	1.32281	10.322	1.32288
0.913	1.34479	100.351	1.35185

**Figure 1.** Trapped-mode wavenumbers,  $kd$ , plotted against  $a/d$  for three ellipses:  $-----$ ,  $b/a = 0.5$ ;  $—$ ,  $b/a = 1$ ;  $- \cdot -$ ,  $b/a = 1.5$ .

different truncation parameters with accurate values obtained using the method of Callan *et al.* (1991).

An example of the results that are obtained from our method is given in figure 1. Figure 2 (*a, b*) shows shaded contour plots of  $\phi$  for these modes, normalized so that the maximum value of  $\phi$  on the body is 1. Symmetric (figure 2*a*) modes are shown, while the antisymmetric ones appear in figure 2(*b*).

### 3.2. Basic properties

Let

$$\rho_l = \lim_{\zeta \rightarrow Z_l^-(x)} \rho(x, \zeta), \quad \rho_u = \lim_{\zeta \rightarrow Z_u^+(x)} \rho(x, \zeta) \quad (3.5a, b)$$

be the fluid densities immediately below and above the cat's-eyes. Finally let  $\rho_0$  and  $N_0$  be the constant values of the density and the vorticity inside the cat's-eyes, so that

$$(\rho(x, \zeta), \phi_{\zeta\zeta}(x, \zeta)) = (\rho_0, N_0) \quad \text{for} \quad Z_l(x) < \zeta < Z_u(x). \quad (3.6)$$

The Reynolds number  $Re$  is defined by  $u_\tau H/\nu$  ( $\nu$  is the kinematic viscosity), the length given in wall units is denoted by  $( )_+$ , and the Prandtl number  $Pr$  is set equal to 0.7. In (2.1) and (2.2),  $\tau_{ij}$  and  $\tau_j^\theta$  are

$$\tau_{ij} = (\overline{\overline{u_i u_j}} - \overline{u_i} \overline{u_j}) + \overline{(\overline{u_i u_j^{SGS}} + u_i^{SGS} \overline{u_j})} + \overline{u_i^{SGS} u_j^{SGS}}, \quad (3.7a)$$

$$\tau_j^\theta = (\overline{\overline{u_j \theta}} - \overline{u_j} \overline{\theta}) + \overline{(\overline{u_j \theta^{SGS}} + u_j^{SGS} \overline{\theta})} + \overline{u_j^{SGS} \theta^{SGS}}. \quad (3.7b)$$

#### 3.2.1. Calculation of the terms

The first terms in the right-hand side of (3.5*a*) and (3.5*b*) are the Leonard terms explicitly calculated by applying the Gaussian filter in the  $x$ - and  $z$ -directions in the Fourier space.

The interface boundary conditions given by (2.1) and (2.2), which relate the displacement and stress state of the wall at the mean interface to the disturbance quantities of the



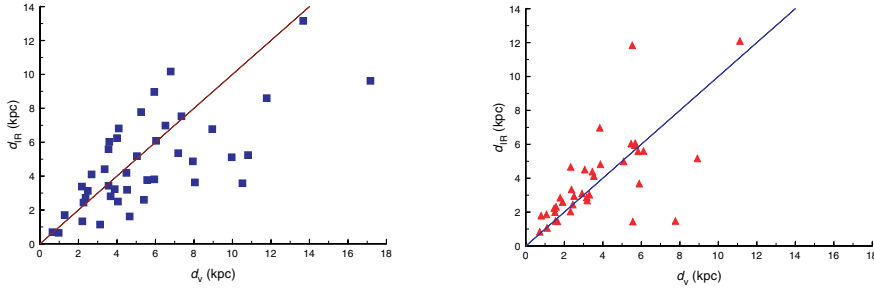


**Figure 2.** Shaded contour plots of the potential  $\phi$  for the two trapped modes that exist for an ellipse with  $a/d = 1.5$ ,  $b/d = 0.75$ . (a) Symmetric about  $x = 0$ ,  $kd = 0.96$ ; (b) antisymmetric about  $x = 0$ ,  $kd = 1.398$ .

flow, can also be reformulated in terms of the transformed quantities. The transformed boundary conditions are summarized below in a matrix form that is convenient for the subsequent development of the theory:

$$Q_C = \begin{bmatrix} -\omega^{-2}V'_w & -(\alpha^t\omega)^{-1} & 0 & 0 & 0 \\ \frac{\beta}{\alpha\omega^2}V'_w & 0 & 0 & 0 & i\omega^{-1} \\ i\omega^{-1} & 0 & 0 & 0 & 0 \\ iR_\delta^{-1}(\alpha^t + \omega^{-1}V''_w) & 0 & -(i\alpha^t R_\delta)^{-1} & 0 & 0 \\ \frac{i\beta}{\alpha\omega}R_\delta^{-1}V''_w & 0 & 0 & 0 & 0 \\ (i\alpha^t)^{-1}V'_w & (3R_\delta^{-1} + c^t(i\alpha^t)^{-1}) & 0 & -(\alpha^t)^{-2}R_\delta^{-1} & 0 \end{bmatrix}. \quad (3.8)$$

$\mathbf{S}^t$  is termed the displacement-stress vector and  $Q_C$  the flow-wall coupling matrix. Subscript  $w$  in (3.8) denotes evaluation of the terms at the mean interface. It is noted that  $V''_w = 0$  for the Blasius mean flow.

### 3.2.2. Wave propagation in anisotropic compliant layers

From (2.1), the fundamental wave solutions to (3.1) and (3.2) for a uniformly thick homogeneous layer in the transformed variables has the form of

$$\boldsymbol{\eta}^t = \hat{\boldsymbol{\eta}}^t \exp[i(\alpha^t x_1^t - \omega t)], \quad (3.9)$$

where  $\hat{\boldsymbol{\eta}}^t = \mathbf{b} \exp(i\gamma x_3^t)$ . For a non-trivial wave, the substitution of (1.7) into (1.3) and (1.4) yields the following determinantal equation:

$$\text{Det}[\rho\omega^2 \delta_{ps} - C_{pqrs}^t k_q^t k_r^t] = 0, \quad (3.10)$$

where the wavenumbers  $\langle k_1^t, k_2^t, k_3^t \rangle = \langle \alpha^t, 0, \gamma \rangle$  and  $\delta_{ps}$  is the Kronecker delta.

## 4. Torus translating along an axis of symmetry

Consider a torus with axes  $a, b$  (see figure 2), moving along the  $z$ -axis. Symmetry considerations imply the following form for the stress function, given in body coordinates:

$$\mathbf{f}(\theta, \psi) = (g(\psi) \cos \theta, g(\psi) \sin \theta, f(\psi)). \quad (4.1)$$

Because of symmetry, one can integrate analytically in the  $\theta$ -direction obtaining a pair

of equations for the coefficients  $f, g$  in (4.1),

$$f(\psi_1) = \frac{3b}{\pi[2(a + b \cos \psi_1)]^{3/2}} \int_0^{2\pi} \frac{(\sin \psi_1 - \sin \psi)(a + b \cos \psi)^{1/2}}{[1 - \cos(\psi_1 - \psi)](2 + \alpha)^{1/2}} d\psi, \quad (4.2)$$

$$\begin{aligned} g(\psi_1) = & \frac{3}{\pi[2(a + b \cos \psi_1)]^{3/2}} \int_0^{2\pi} \left( \frac{a + b \cos \psi}{2 + \alpha} \right)^{1/2} \left\{ f(\psi)[(\cos \psi_1 - b\beta_1)S + \beta_1 P] \right. \\ & \times \frac{\sin \psi_1 - \sin \psi}{1 - \cos(\psi_1 - \psi)} + g(\psi) \left[ \left( 2 + \alpha - \frac{(\sin \psi_1 - \sin \psi)^2}{1 - \cos(\psi_1 - \psi)} - b^2 \gamma \right) S \right. \\ & \left. \left. + \left( b^2 \cos \psi_1 \gamma - \frac{a}{b} \alpha \right) F\left(\frac{1}{2}\pi, \delta\right) - (2 + \alpha) \cos \psi_1 E\left(\frac{1}{2}\pi, \delta\right) \right] \right\} d\psi, \quad (4.3) \end{aligned}$$

$$\alpha = \alpha(\psi, \psi_1) = \frac{b^2[1 - \cos(\psi - \psi_1)]}{(a + b \cos \psi)(a + b \cos \psi_1)}; \quad \beta = \beta(\psi, \psi_1) = \frac{1 - \cos(\psi - \psi_1)}{a + b \cos \psi}. \quad (4.4)$$

## 5. Conclusions

We have shown how integral equations can be used to solve a particular class of problems concerning obstacles in waveguides, namely the Neumann problem for bodies symmetric about the centreline of a channel, and two such problems were considered in detail.

## Appendix A. Boundary conditions

It is convenient for numerical purposes to change the independent variable in (4.1) to  $z = y/\tilde{v}_T^{1/2}$  and to introduce the dependent variable  $H(z) = (f - \tilde{y})/\tilde{v}_T^{1/2}$ . Equation (4.1) then becomes

$$(1 - \beta)(H + z)H'' - (2 + H')H' = H'''. \quad (A 1)$$

Boundary conditions to (4.3) follow from (4.2) and the definition of  $H$ :

$$\left. \begin{aligned} H(0) &= \frac{\epsilon \bar{C}_v}{\tilde{v}_T^{1/2}(1 - \beta)}; & H'(0) &= -1 + \epsilon^{2/3} \bar{C}_u + \epsilon \hat{C}'_u; \\ H''(0) &= \frac{\epsilon u_*^2}{\tilde{v}_T^{1/2} u_P^2}; & H'(\infty) &= 0. \end{aligned} \right\} \quad (A 2)$$

## Appendix B.

A simple sufficient condition for the method of separation of variables to hold for the convection problem is derived. This criterion is then shown to be satisfied for the ansatz described by (3.27), thus justifying the approach used in § 3. The basic ingredient of our argument is contained in the following estimate for a Rayleigh–Ritz ratio:

LEMMA 1. *Let  $f(z)$  be a trial function defined on  $[0, 1]$ . Let  $A_1$  denote the ground-state eigenvalue for  $-d^2g/dz^2 = Ag$ , where  $g$  must satisfy  $\pm dg/dz + \alpha g = 0$  at  $z = 0, 1$  for*

some non-negative constant  $\alpha$ . Then for any  $f$  that is not identically zero we have

$$\frac{\alpha(f^2(0) + f^2(1)) + \int_0^1 \left(\frac{df}{dz}\right)^2 dz}{\int_0^1 f^2 dz} \geq \Lambda_1 \geq \left(\frac{-\alpha + (\alpha^2 + 8\pi^2\alpha)^{1/2}}{4\pi}\right)^2. \quad (\text{B } 1)$$

Before proving it, we note that the first inequality is the standard variational characterization for the eigenvalue  $\Lambda_1$ .

**COROLLARY 1.** *Any non-zero trial function  $f$  which satisfies the boundary condition  $f(0) = f(1) = 0$  always satisfies*

$$\int_0^1 \left(\frac{df}{dz}\right)^2 dz. \quad (\text{B } 2)$$

### Acknowledgements

We would like to acknowledge the useful comments of a referee concerning the solution procedure used in § 5. A. N. O. is supported by SERC under grant number GR/F/12345.

### References

- Bearman, P.W. & Graham, J.M.R. 1980, *J. Fluid Mech.* 99, 225  
 Callan, M., Linton, C.M. & Evans D.V. 1991, *J. Fluid Mech.* 229, 51  
 Dennis, S.C.R. 1985, in: X. Soubbaramayer & J.P. Boujot (eds.), *Ninth Intl. Conf. on Numerical Methods in Fluid Dynamics*, Lecture Notes in Physics (Heidelberg: Springer), vol. 218, p. 23  
 Figer, D.F., Najarro, F., Gilmore, D., Morris, M., Kim, S.S., Serabyn, E., McLean, I.S., Gilbert, A.M., Graham, J.R., Larkin, J.E., Levenson, N.A., Teplitz, H.I. 2002, *ApJ* 581, 258  
 Hwang, L.-S. & Tuck, E.O. 1970, *J. Fluid Mech.* 42, 447  
 Keller, H.B. 1977 in: P.H. Rabinovich (ed.), *Applications of Bifurcation Theory* (Academic), p. 359  
 Koch, W. 1983, *J. Sound Vib.* 88, 233  
 Krabbe, A., Genzel, R., Eckart, A., Najarro, F., Lutz, D., Cameron, M., Kroker, H., Tacconi-Garman, L. E., Thatte, N., Weitzel, L., Drapatz, S., Geballe, T., Sternberg, A., Kudritzki, R.-P. 1995, *ApJ* (Letters) 447, L95  
 Lee, J.-J. 1971, *J. Fluid Mech.* 45, 375  
 Linton, C.M. & Evans, D.V. 1992, *Phil. Trans. R. Soc. Lond.* A338, 325  
 Martin, P.A. 1980, *Q. J. Mech. Appl. Maths* 33, 385  
 Rogallo, R.S. 1981, *NASA Tech. Mem.* 81835.  
 Ursell, F. 1950, *Proc. Camb. Phil. Soc.* 46, 141  
 van Wijngaarden, L. 1968, *J. Engng Maths* 2, 225  
 Williams, J.A. 1964, PhD thesis, University of California, Berkeley.

### Discussion

MASSEY: Im wondering if you have considered the expected intrinsic dispersion in absolute magnitude of WRs – if you consider the (large) mass range that becomes an early WN or late WC according to the evolutionary models, wouldnt you expect a large dispersion in  $M_v$ ?

VAN DER HUCHT: Indeed, we will be always left with some intrinsic scatter in  $M_v$  due to mass differences within the same spectral subtype. But in my opinion, the current large

dispersion is for a large fraction due to uncertainties of the adopted distances of open clusters and OB associations.

WALBORN: I think that the scatter in WNL absolute magnitudes is dominated by intrinsic spread rather than errors. In the LMC, one finds a range of 5 to nearly 8. This in turn likely reflects different formation channels: mass-transfer binaries, post-RSG, and extremely massive stars in giant H II regions.

VAN DER HUHT: As said above, there is likely to be intrinsic scatter. But, I wonder whether a scatter of 3 magnitudes perhaps reflects undetected multiplicity.

MAÍZ-APELLÁNIZ: I could not agree more with your comment on the need for an updated catalogue of O-type stars (as a follow up of that of Garmany *et al.* 1982). We are currently working on precisely that (see our poster, these Proceedings) and we will soon make it available.

VAN DER HUHT: Wonderful.

KOENIGSBERGER: Is the ratio WR/O-stars in clusters similar or different from this ratio for the field stars?

VAN DER HUHT: I think it is different because incompleteness among field stars is even larger than that among cluster stars. But perhaps it should also be different because WR stars are older and could have drifted away from clusters, more than O-type stars.

GIES: How many of the WR stars in your catalogue might be low mass objects?

WALBORN: Comment: PN central stars in the WR sample would be only [WC].

VAN DER HUHT: Among the WR stars in our VIIth Catalogue we doubt only one: WR109 (V617 Sgr), which is a peculiar object (not even a [WR] central star of a PN). All other stars in our catalogue are true massive Population I WR stars, and properly classified as such. We have not listed known Population II [WC] objects, as we did separately in our VIth Catalogue (van der Hucht *et al.* 1981). [WN] objects are not known to exist, see the comment by Nolan.

ZINNECKER: Are all Galactic WR stars in open clusters and OB association or are there many WR stars in the field?

VAN DER HUHT: See the VIIth WR catalogue (van der Hucht 2001): of the listed 227 Galactic WR stars, only 53 are in open clusters and OB associations, or believed to be. The other 184 are supposedly field stars.

